

Controlled synthesis of ZnO nanorods and layered double hydroxide nanocomposites using a composition-modulated seed layer

Seong-Ho Baek^a and Il-Kyu Park^{b,*}

^aEnergy Research Division, Daegu Gyeongbuk Institute of Science & Technology (DGIST), Daegu 711-873, South Korea

^bDepartment of Materials Science and Engineering, Seoul National University of Science and Technology, Seoul 139-743, South Korea

We report the structural evolution of ZnO nanorods (NRs) and ZnAl layered double hydroxide (LDH) hybrid nanostructures fabricated by a simple hydrothermal method. The morphology of the hybrid nanostructures depended on the composition of the single seed layer of Al-alloyed ZnO (AZO) with different ratios of Al and Zn, which was grown by atomic layer deposition method. When the AZO seed layer was Al rich, the surface was mainly covered by the ZnAl-LDH structures. As the Al content decreased, the ZnO NRs dominated the hybrid nanostructures and pure ZnO NRs were finally formed when Zn-rich AZO or ZnO layers were used as a seed layer. A morphological evolution mechanism is suggested based on the different solubility of the sacrificial AZO seed layers, which depends on the Al content because the isoelectric point is larger in the ZnO than in the Al₂O₃.

Key words: ZnAl-layered double hydroxide, ZnO nanorod, Hybrid structure, Nanocomposite.

Introduction

Low-dimensional nanostructures have received great attention for a wide variety of applications and for their novel physical properties. One and two-dimensional nanostructures in particular have been regarded as good candidates for device applications due to advantages arising from their shapes [1-3]. Nanorod (NR), nanowire, and nanotube one-dimensional nanostructures based on inorganic or organic material have been investigated widely [2,3]. ZnO NRs can be grown by a simple low-temperature solution process on any substrate, regardless of its area, shape, and morphology. They have been considered for potential applications in piezotronics, optoelectronics, and resilient energy systems due to attractive features such as wide band gap semiconducting, piezoelectric, and photoelectric properties [4-8].

In the case of two-dimensional nanostructures, carbon-based graphene or chalcogenide-based nanosheets are widely investigated for their drastic changes in electrical or optical properties with the number of sheets [1]. Layered double hydroxide (LDH) structures are another fascinating two-dimensional system [9-13]. The LDH structure is made of ionic lamellar materials belonging to the group of anionic clays. The basic structure of LDH is brucite-like layers which are composed of $[M^{II}_{(1-x)}M^{III}_{(x)}(OH)_2][A^{n-}_{x/n} \cdot mH_2O]$ ($M^{II} = Ca, Zn, Mg, Ni$; $M^{III} = Al, Cr, Ga$; $A^{n-} = CO_3^{2-}, Cl^-, NO_3^-$,

CH_3COO^-) [9-13]. Two different cations, M^{II} and M^{III} , occupy the octahedral holes in a brucite-like layer and A^{n-} anions, such as nitrates, carbonates, sulfates, phosphates, and hydroxyl groups are located in the hydrated interlamellar galleries [9-13]. Because many combinations of ionic elements are allowed in the structure, LDHs have been regarded as an excellent building block for many applications, such as physical, optical, or chemical sensors, catalysts, absorbents, electrochromic devices, and electrodes for energy storage devices [9-15]. If the ZnO NRs and LDH structures could be hybridized, novel complementary effects originating from one and two-dimensional nanostructures are expected. Recently, our group reported the control of hybrid nanostructures of ZnO NRs and ZnAl-LDHs by controlling the thickness of Al₂O₃ and ZnO double seed layers [16]. The morphology of the hybrid nanostructures varied very sensitively depending on the thickness of the Al₂O₃ and ZnO layers [16]. A more feasible way to fabricate the hybrid structure is needed for a practical, simple, and cost-effective way to extend its applications. In this paper, we report on a novel approach for controlling the morphology of ZnAl-LDH and ZnO NR hybrid nanostructures on Si substrate using Al-alloyed ZnO (AZO) layers with various Al contents.

Experimental Procedure

Three kinds of seed layers were deposited on glass and silicon wafers using an atomic layer deposition system (NCD, LUCIDA D-100): ZnO, Al-alloyed ZnO

*Corresponding author:
Tel : +82-2-970-6349
Fax: +82-2-973-6657
E-mail: pik@seoultech.ac.kr

(AZO) with different Al content, and Al₂O₃. diethylzinc (DEZn), water (H₂O), and trimethylaluminum (TMAI) were used as precursors for the Zn, O, and Al, respectively. High-purity N₂ was used as a carrier gas and to remove byproducts. A DEZn-H₂O cycle was used for the ZnO deposition, and TMAI-H₂O was used for the Al₂O₃ layer. To fabricate the AZO layers with different Al contents, TMAI-H₂O and DEZn-H₂O cycles were performed with cycle ratios of 1 : 19, 1 : 9, and 1 : 4, and the resulting layers are referred to as AZO-1/19, AZO-1/9, and AZO-1/4, respectively. All thin films were deposited on substrates with 6-nm thickness.

ZnAl-LDH and ZnO NR hybrid nanostructures were formed on the various seed layers deposited on Si substrate. As a precursors for hydrothermal synthesis, we used zinc nitrate hexahydrate (Zn(NO₃)₂·6H₂O, 99.99% purity, Sigma-Aldrich) and hexamethylenetetramine ((HMT; C₆H₁₂N₄), Sigma-Aldrich). A mixed solution of 60 mM zinc nitrate hexahydrate and HMT in deionized (DI) water was prepared and followed by dipping the seed layer-deposited substrates into the solution. The solution was kept at 90 °C for 2 hrs during the growth of ZnO NR and ZnAl-LDH layers. All samples were rinsed in flowing DI water for 10 min to completely remove the residues, especially the free standing ZnO crystals, from the samples.

The structural investigations were carried out by scanning electron microscopy (SEM, Hitachi S-4800) and transmission electron microscopy (TEM, Hitachi HF-3300) for the cleaved ZnAl-LDH and ZnO NR structures. To prepare the TEM samples, a focused ion beam (FIB, Hitachi NB 5000) system was used. To study the crystalline structures of the nanostructures were investigated by X-ray diffraction (XRD, PANalytical Empyrean). The transmittance spectra of the seed layers grown on glass substrate were measured by a UV-Vis-NIR spectrophotometer using an integrating sphere (Cary 5000, Agilent). Photoluminescence (PL) was measured to investigate the optical properties of the ZnAl-LDH and ZnO NRs by using a He-Cd 325 nm laser at room temperature.

Results and Discussion

To investigate the change in the bandgap with varying ALD precursor, the optical absorption spectra were measured for the pure ZnO and AZO thin films with different Al composition corresponding to AZO-1/19, AZO-1/9, and AZO-1/4 samples. The dependence of $(\alpha hv)^2$ on the photon energy (hv) is plotted in Fig. 1, where α is the absorption coefficient of the film [17]. The optical band gaps (E_g) of the samples were estimated by extrapolation of the linear regions of the optical absorption edges on the $(\alpha hv)^2$ vs. hv curves [17]. In the case of the pure ZnO thin film, the measured bandgap energy was 3.28 eV, which is very

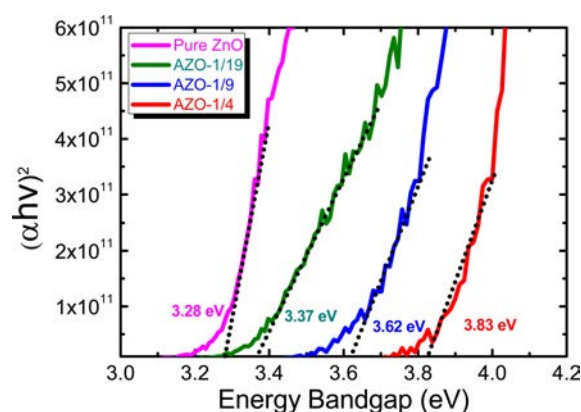


Fig. 1. Optical absorption spectra of ZnO, Al₂O₃, and AZO films with different compositions deposited on quartz glass by ALD.

similar to the well-known value. The optical band gap was clearly blue-shifted with increasing Al₂O₃ cycle ratios during the ALD deposition. The band gap energy of the AZO increased from 3.37 to 3.83 eV when the Al₂O₃/ZnO cycle ratio increased from 1/19 to 1/4. The Al concentration of the AZO thin film can be estimated from the relation between the band gap energy versus the Al concentration x_{Al} as E_g (eV) = 3.26 + 0.0749 x_{Al} [18]. The estimated Al contents of the AZO-1/19, AZO-1/9, and AZO-1/4 samples were 1.46, 4.79, and 7.58%, respectively. Even though the Al composition in the AZO thin films does not show a linear relation with the Al₂O₃/ZnO cycle ratio, it clearly increases with the cycle ratios. Therefore, we can conclude that the AZO layers have different Al content.

Fig. 2 shows top-view and cross-sectional SEM images of the synthesized ZnAl-LDH and ZnO NRs grown on the various seed layers. Figs. 2(a-b) clearly show that flake-like structures occurred when the pure Al₂O₃ was used as a seed layer. These structures are considered to be a ZnAl-LDH phase in which Al³⁺ cations are isomorphously substituted by divalent Zn²⁺ cations. The Al³⁺ cations are supplied from the dissolved Al₂O₃ seed layer because the Al₂O₃ has been known to act as a sacrificial seed layer in the hydrothermal solution [19]. As the Al content decreases (AZO-1/4), the size of the ZnAl-LDH structure decreases slightly, as shown in Figs. 2(c-d). This is attributed to the reduction of the Al hydroxide concentration on the growth surfaces, which were dissolved from the seed layers. As the Al content in the AZO seed layer decreases further (AZO-1/9), a ZnO NR structure with a hexagonal cross section starts to appear between the ZnAl-LDH flakes, as shown in Figs. 2(e-f). For AZO-1/19, the ZnO NR structure predominantly formed on the surface, as shown in Figs. 2(g-h). The reduction of the ZnAl-LDH over the ZnO NRs with decreasing Al content can be attributed to reduction in the Al hydroxide species in the solution near the growth front. When the pure ZnO was used as a seed layer, as shown

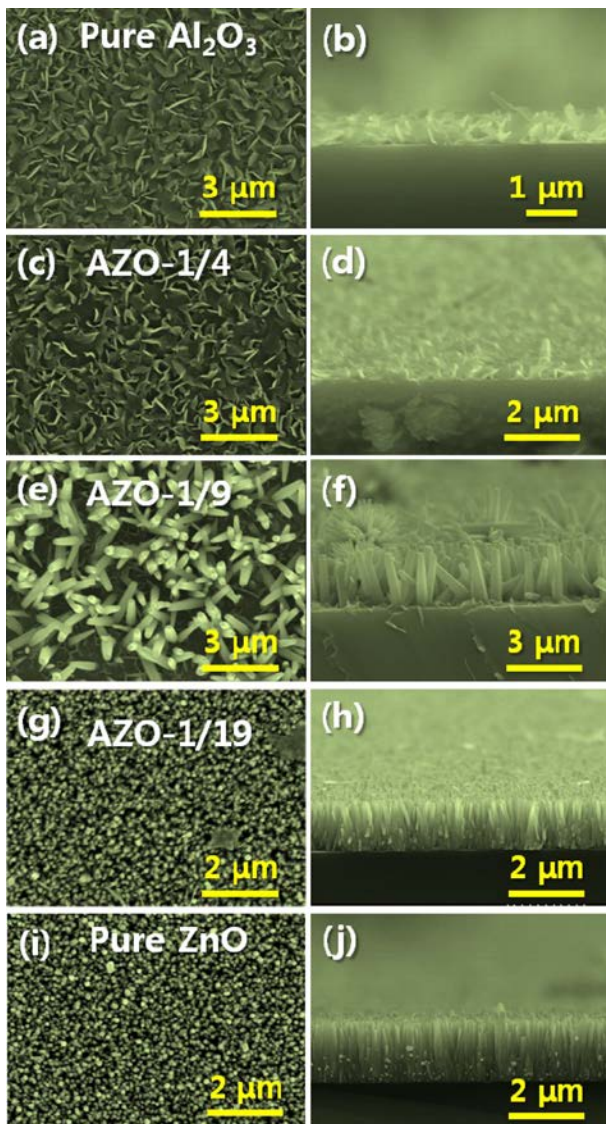


Fig. 2. FE-SEM images of ZnO NR and ZnAl-LDH structures on *n*-Si (100) substrates with different compositions of AZO seed layers: (a) and (b) pure Al₂O₃; (c) and (d) AZO-1/4; (e) and (f) AZO-1/9; (g) and (h) AZO-1/19; (i) and (j) pure ZnO.

in Figs. 2(i-j), no ZnAl-LDH structure was observed, and the surface was completely covered by the ZnO

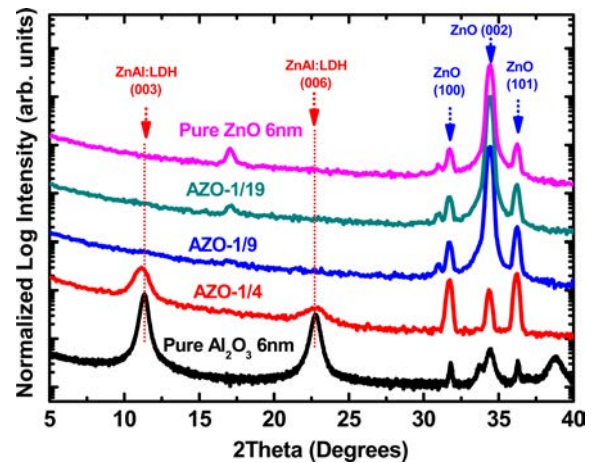


Fig. 3. Normalized θ - 2θ XRD patterns of ZnO NR and ZnAl-LDH structures on *n*-Si (100) substrates with different compositions of the AZO seed layer.

NRs because of the lattice-matched ZnO buffer layer on the substrate. This indicates that the Al content in the AZO seed layer plays a critical role in determining the morphological transition of the ZnAl-LDH and ZnO NR hybrid nanostructures.

XRD measurement was conducted to investigate the structural evolution of the ZnAl-LDH and ZnO NR hybrid composites. As shown in Fig. 3, the XRD pattern of the sample grown on an Al₂O₃ layer shows two strong diffraction peaks corresponding to (003) and (006) reflections of a crystalline ZnAl-LDH phase with R-3m rhombohedral symmetry [10, 13, 16]. The presence of (003) and (006) reflections confirms the formation of a layered structure of the ZnAl-LDH materials. With decreasing Al content in the AZO seed layers, however, the diffraction peaks from the ZnAl-LDH disappear drastically, and other phases start to appear. The new peaks at $2\theta = 31.87^\circ$, 34.45° , and 36.31° correspond to the (100), (002), and (101) planes of the wurtzite ZnO crystal, respectively. Therefore, the mixed ZnAl-LDH and ZnO NR structures are present on the surface when the Al/Zn ratio decreases to 1/9. However, as the Al/Zn ratio decreases further to 1/19, diffraction peaks from only the ZnO NRs are observed.

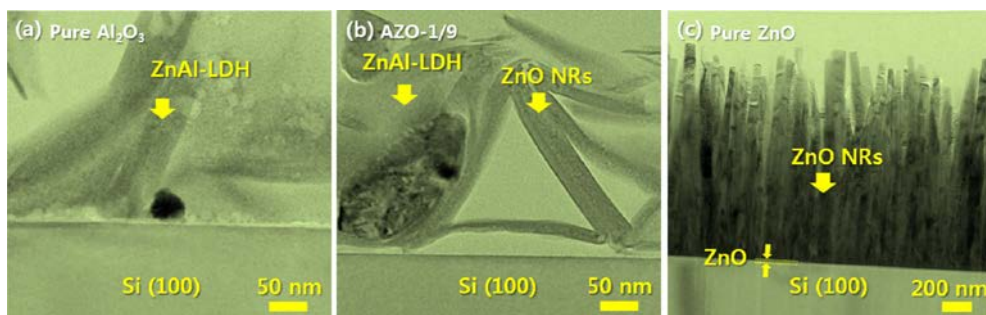


Fig. 4. Cross-sectional HR-TEM images of the of ZnO NR and ZnAl-LDH structures on different seed layers: (a) pure Al₂O₃, (b) AZO-1/9, and (c) pure ZnO.

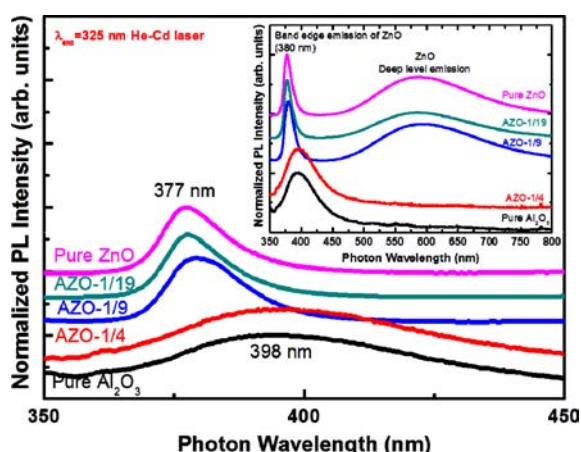


Fig. 5. Normalized room temperature PL spectra of ZnO NR and ZnAl-LDH hybrid structures on *n*-Si (100) substrates with different compositions of the AZO seed layer. Inset shows PL spectra for full wavelength range.

These results are in good agreement with the morphological evolutions observed by SEM shown in Fig. 2. The fabricated ZnAl-LDHs and ZnO NRs also had good phase purity and crystallinity.

Microstructure of the ZnO NR and ZnAl-LDH hybrid structures were investigated by cross-sectional TEM as shown in Fig. 4. The microstructure changes from ZnAl-LDHs to ZnO NRs, depending on the composition of the AZO seed layers. In the case of AZO-1/9, mixed structures of ZnO NR and ZnAl-LDH clearly occur on the surface according to the SEM and XRD measurements. As shown in Fig. 4(b), the ZnO NRs are not attached to the surface which is obviously different from the ZnO NRs grown on the ZnO seed layers. This is attributed to the AZO seed layer dissolving while the ZnO seed layer is maintained, as shown in Fig. 4(c). The remaining ZnO seed layers are lattice-matched with the ZnO NRs and result in vertically aligned growth of ZnO NRs.

The optical properties of the ZnO NR and ZnAl-LDH hybrid structures, the room-temperature PL spectra were measured as shown in Fig. 5. When the Al/Zn ratio is smaller than 1/9 (i.e., AZO-1/9, AZO-1/19, and pure ZnO samples), the PL spectra show dual emission bands with a sharp asymmetric peak around 377 nm and a broad band around 600 nm, as shown in the inset of Fig. 5. This feature is very similar to that of ZnO nanostructures synthesized by a wet chemistry method [20, 21]. The emission peaks in the UV and visible wavelength ranges correspond to the band-edge emission and the ensemble of deep level-related emission from the ZnO crystal lattice, respectively [20, 21]. Even though the AZO-1/9 sample consists of mixed structures of ZnO NRs and ZnAl-LDH, the PL spectrum shows an emission peak from only the ZnO NRs. This is due to the much stronger emission from the ZnO NRs than from the ZnAl-LDHs dominating the emission spectrum. As shown in Fig. 5, the emission spectra from the AZO-1/9 and AZO-1/19 show asymmetric shoulders at longer wavelength which originates from the ZnAl-LDHs. For the AZO-1/4 and pure Al_2O_3 , a single emission peak occurs around 398 nm, which originated from the ZnAl-LDH structures [16, 22]. These results are consistent with the structural investigations, where only ZnAl-LDH structures were found when the seed layer was AZO-1/4 and pure Al_2O_3 .

Based on the structural and optical results, a schematic diagram of the morphological evolution mechanism of the ZnO NR and ZnAl-LDH hybrid nanostructures with different Al content in the seed layer is shown in Fig. 6. In the reaction, the hydroxide ions in the solution play critical roles in the structural evolution of the hybrid nanostructures by providing O sources for the hydroxide reaction of ZnO NRs and dissolving the AZO seed layers, depending on the Al content. The hydroxide ions are formed by the decomposition of ammonia generated from the HMT

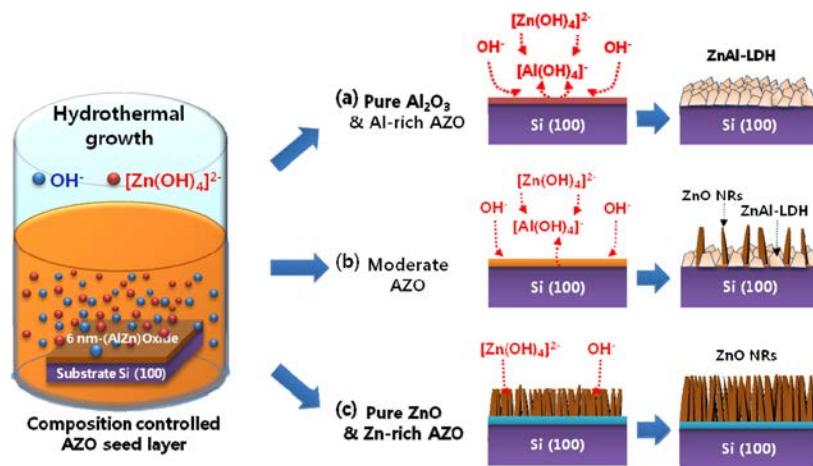
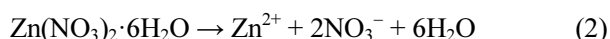


Fig. 6. Schematic diagram for the evolution of the ZnO NR and ZnAl-LDH hybrid structures with different compositions of the AZO seed layer.

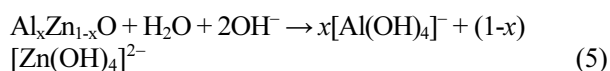
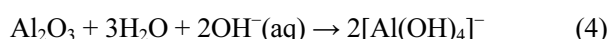
$((\text{CH}_2)_6\text{N}_4)$ [23]:



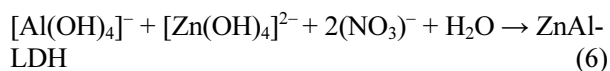
The hydride ions contribute to growing the ZnO NRs on the ZnO or Zn-rich AZO seed layers by the following reactions:



At the same time, the hydride ions dissolve the Al_2O_3 or Al-rich AZO seed layers by the following reactions:



The ZnAl-LDHs are then formed by hydrothermal reactions in the aqueous solutions, as described in previous studies [24]:



The pure Al_2O_3 and Al-rich AZO seed layers are dissolved by the hydride ions according to reactions (4) and (5). They provide hydroxoaluminate ions at the growth front of the substrate to form the ZnAl-LDHs. As the Al content in the AZO seed layers decreases, the seed layers are rarely dissolved by the hydride ions because the isoelectric point value of the ZnO is 9.8, while that of the Al_2O_3 is 7.6 [25, 26]. This indicates that the ZnO is expected to crystallize due to the hydrolysis of Zn salts and is more stable than the Al_2O_3 in OH^- -rich basic solutions. Therefore, the ZnO or Zn-rich AZO layers remain without dissolution and act as a seed layer for the formation of ZnO NRs, as shown in Figs. 6(b-c). However, the Al_2O_3 or Al-rich AZO seed layers are dissolved into the solution by OH^- ions to form the ZnAl-LDH structures, as shown in Fig. 6(a). In this way, the morphology of the ZnO NR and ZnAl-LDH hybrid nanostructures could be controlled successfully by using a composition-modulated single AZO seed layer.

Conclusions

In conclusion, we have investigated the structural evolution of ZnAl-LDH and ZnO NR structures by controlling the Al composition in a single AZO seed layer. The composition-modulated AZO seed layer was fabricated by changing the $\text{Al}_2\text{O}_3/\text{ZnO}$ cycle ratio in the ALD system. The structural investigations by SEM, XRD and TEM results showed that the formation of the ZnO NR and hybrid structures could be controlled

by the Al content in the AZO seed layers. When pure Al_2O_3 or Al-rich AZO were used as seed layers, ZnAl-LDH structures were mostly formed on the surface. As the Al content decreased, mixed structures of ZnO NR and ZnAl LDH were formed. However, when the Zn-rich AZO and ZnO seed layers were used, the ZnO NRs dominated on the surface. The morphological evolution mechanism was explained based on the dissolution of the AZO seed layers depending on the composition because the isoelectric point of the ZnO was larger than that of Al_2O_3 . Therefore, we could successfully control the morphology of the ZnO NR and ZnAl-LDH hybrid nanostructures by using a composition-modulated AZO seed layer.

Acknowledgments

The authors especially thanks to Mr. Gwang-Hee Nam (Yeungnam University) for assistance with the experiments. This research was supported by the Basic Science Research Program (NRF-2014R1A2A1A11054154) through the National Research Foundation of Korea, and by the DGIST R&D Program (No. 17-EN-01) funded by the Ministry of Science, ICT and Future Planning of the Korean government.

References

1. G.R. Bhimanapati, Z. Lin, V. Meunier, Y. Jung, J. Cha, S. Das, D. Xiao, Y. Son, M.S. Strano, V.R. Cooper, L. Liang, S.G. Louie, E. Ringe, W. Zhou, S.S. Kim, R. R. Naik, B.G. Sumpter, H. Terrones, F. Xia, Y. Wang, J. Zhu, D. Akinwande, N. Alem, J.A. Schuller, R.E. Schaak, M. Terrones, and J.A. Robinson, *ACS Nano* 9 (2015) 11509-11539.
2. Z.L. Wang, *Nano Today* 5 (2010) 512-514.
3. Y. Xia, P. Yang, Y. Sun, Y. Wu, B. Mayers, B. Gates, Y. Yin, F. Kim, and H. Yan, *Adv. Mater.* 15 (2003) 353-389.
4. S. Xu and Z.L. Wang, *Nano Res.* 4 (2011) 1013-1099.
5. Z.L. Wang and J. Song, *Science* 312 (2006) 242-246.
6. D.Y. Jung, S.H. Baek, M.R. Hasan, and I.K. Park, *J. All. Comp.* 641 (2015) 163-169.
7. G.H. Nam, S.H. Baek, C.H. Cho, and I.K. Park, *Nanoscale* 6 (2015) 11653-11658.
8. C. Soci, A. Zhang, B. Xiang, S.A. Dayeh, D.P.R. Aplin, J. Park, X.Y. Bao, Y.H. Lo, and D. Wang, *Nano Lett.* 7 (2007) 1003-1009.
9. J.H. Koo and B.W. Lee, *J. Ceram. Process. Res.* 18 (2017) 156-160.
10. A.I. Khan, A. Raghavan, B. Fong, C. Markland, M. O'Brien, T.G. Dunbar, G.R. Williams, and D. O'Hare, *Ind. Eng. Chem. Res.* 48 (2009) 10196-10205.
11. X. Zhao, F. Zhang, S. Xu, D.G. Evans, and X. Duan, *Chem. Mater.* 22 (2010) 3933-3942.
12. Q. Wang and D. O'Hare, *Chem. Rev.* 112 (2012) 4124-4155.
13. W. Bao, J. Wang, Q. Wang, D. O'Hare, and Y. Wan, *Sci. Rep.* 6 (2016) 26738.
14. M. Gong, Y. Li, H. Zhang, B. Zhang, W. Zhou, J. Feng, H. Wang, Y. Liang, Z. Fan, J. Liu, and H. Dai, *Energy Environ. Sci.* 7 (2014) 2025-2032.
15. X. Liu, A. Zhou, Y. Dou, T. Pan, M. Shao, J. Han, and M.

- Wei, *Nanoscale* 7 (2015) 17088-17095.
17. S.H. Baek, G.H. Nam, and I.K. Park, *RSC Adv.* 5 (2015) 59823-59829.
18. J. Tauc, *Mater. Res. Bull.* 3 (1968) 37-46.
19. Q. Hou, F. Meng, and J. Sun, *Nanoscale Res. Lett.* 8 (2013) 144.
20. X. Guo, S. Xu, L. Zhao, W. Lu, F. Zhang, D.G. Evans, and X. Duan, *Langmuir* 25 (2009) 9894-9897.
21. G.H. Nam, S.H. Baek, and I.K. Park, *J. All. Comp.* 613 (2014) 37-41.
22. D. Li, Y. Leung, A. Djurišić, Z. Liu, M. Xie, S. Shi, S. Xu, and W. Chan, *Appl. Phys. Lett.* 85 (2004) 1601-1603.
23. Z. Zhang, G. Chen, and K. Xu, *Ind. Eng. Chem. Res.* 52 (2013) 11045-11049.
24. X. Yan, Z. Li, R. Chen, and W. Gao, *Cryst. Growth Des.* 8 (2008) 2406-2410.
25. J. Liu, X. Huang, Y. Li, K.M. Sulieman, X. He, and F. Sun, *J. Phys. Chem. B* 110 (2006) 21865-21872.
26. J. Zhai, X. Tao, Y. Pu, X.F. Zeng, and J.F. Chen, *Appl. Surf. Sci.* 257 (2010) 393-397.
27. C. Lei, X. Zhu, Y. Le, B. Zhu, J. Yu, and W. Ho, *RSC Adv.* 6 (2016) 10272-10279.